



Groundwater Circulation and Origin of Salinity in a Multi-aquifer System: The Gohar-Zamin Mining Area, Iran

Mohammad Javad Gharaat¹ · Zargham Mohammadi¹ · Amin Assari² · Fereidoun Rezanezhad³

Received: 19 June 2021 / Accepted: 7 October 2022 / Published online: 19 October 2022
© The Author(s) under exclusive licence to International Mine Water Association 2022

Abstract

Determining the origin of groundwater in active and unstable mining environments has proven quite challenging. We evaluated the origin and salinity of the groundwater using major/minor ions, ²H and ¹⁸O stable isotopes, and ³H and ¹⁴C radioisotopes. Samples were collected from a multi-aquifer system including three distinct aquifers: an upper alluvial aquifer (UAA), a lower alluvial aquifer (LAA), and a hard-rock aquifer (HRA). The water facies for most of the samples were Na-Cl with total dissolved solid concentrations ranging from 1.1 g L⁻¹ in the freshwater of the Kheirabad aquifer (KhA), 148.8 g L⁻¹ in the brines of the HRA, and 321 g L⁻¹ in a salt playa. The unique ionic relationships between the ions imply the salinity mainly originates from halite dissolution. Moreover, the groundwater of HRA and LAA was altered by reverse cation exchange. Although the stable isotope data suggested a modern meteoric water source for the KhA samples, the UAA, LAA, and HRA groundwaters were significantly enriched relative to the local meteoric water line. Dating with ³H and ¹⁴C radioisotopes confirmed the characteristic differences between the aquifers with ages of 6200 (UAA), 18,000 (LAA), and 27,500 years (HRA), which ultimately supported their varied origins. Consequently, a regional conceptual flow model was developed based on the geological settings, stratigraphic evidence, hydrochemistry, and isotopic properties, which suggests that the UAA, LAA, and HRA were due to three transgressions of inland lakes 6200, 18,000, and 27,500 ago, respectively.

Keywords Hard-rock aquifer · Groundwater age dating · Isotopes · Open mine · Hydrogeology

Introduction

Mining and field operations in open-pit mines, where extraction depths are typically below local groundwater levels, are significantly affected by groundwater flow and circulation.

Various issues including slope stability, reduction of mining efficiency, demolition of mine-based equipment, and unsafe working conditions can all occur when groundwater flows into an open-pit mine (Ahmadi et al. 2018; Assari 2019; Heidari-Nejad et al. 2017; Jahanshahi and Zare 2017). Evaluating the origin of groundwater and its salinity mechanisms are some of the fundamental ways to improve both the management and regulation of mining activities (Assari 2019; Heidari-Nejad et al. 2017).

Understanding the processes controlling the evolution of hydrochemical and isotopic properties of groundwater in a complex subsurface system is important in identifying the origin of groundwater (Argamasilla et al. 2017; Mohammadi et al. 2012; Wang and Jiao 2012; Wen et al. 2019) and its hydrochemical evolution (Owen and Cox 2015) using hydrochemical and isotopic techniques (Li et al. 2018, 2019a). A combination of evidence and indexes such as major and minor ions, stable isotopes of water (e.g. ²H and ¹⁸O), and radioisotopes (e.g. ³H and ¹⁴C) have been simultaneously applied to distinguish the origin of groundwater and its salinity sources (Gue et al. 2015; Wang and Jiao

✉ Zargham Mohammadi
zmohammadi@shirazu.ac.ir

Mohammad Javad Gharaat
vahid.gharaat@gmail.com

Amin Assari
Assari1985@gmail.com

Fereidoun Rezanezhad
frezanezhad@uwaterloo.ca

¹ Department of Earth Sciences, Shiraz University, Shiraz 7146713565, Iran

² Gohar-Zamin Iron Ore Co, Gol-Gohar Industrial and Mining Complex, Km 50 Sirjan-Shiraz Rd, Sirjan, Kerman, Iran

³ Ecohydrology Research Group, Water Institute and Department of Earth and Environmental Sciences, University of Waterloo, Waterloo, Canada

2012; Yu et al. 2019). Analyses of major and minor elements and their ionic ratios (e.g. bromine (Br^-)/chloride (Cl^-) and sodium [Na^+]/ Cl^-) are well-known approaches to identify the groundwater salinization sources, such as seawater intrusion (Argamasilla et al. 2017; Eggenkamp et al. 2019), dissolution of evaporites (Gue et al. 2015), oil-field and thermal brines (Alçiçek et al. 2018; Yu et al. 2019), deep-basin brines (Heidari-Nejad et al. 2017; Khaska et al. 2013), and anthropogenic activities (Li et al. 2019b; Prasanna et al. 2012; Scheiber et al. 2016). Stable isotopes of water such as ^2H and ^{18}O have also been extensively used to distinguish local meteoric water from groundwater systems with distinctive origins (Alçiçek et al. 2018; Montcoudiol et al. 2015; Zhao et al. 2017), and to assess the hydrochemical processes, such as evaporation, mixing, and rock-water interaction (Bagheri et al. 2014a, b; Chen et al. 2020; Eissa et al. 2018). Radioisotopes such as ^3H and ^{14}C with half-lives of 12.32 and 5730 years, respectively, have also been widely used for dating groundwater and differentiating old (paleo-water) from modern groundwater (Bourke et al. 2014; Scheiber et al. 2015; Wang and Jiao 2012).

This study focused on groundwater circulation and the origin of salinity in a multi-aquifer system in the Gohar-Zamin iron mine (pit no. 3), an open-pit mine that is dealing with groundwater incursions from both the walls and bottom of the pit (Fig. 1a). This groundwater causes extensive problems for the extraction of iron ore; a large volume of saline water ($7700 \text{ m}^3 \text{ day}^{-1}$) with an average electrical conductivity (EC) of $120,000 \mu\text{S cm}^{-1}$ must be pumped out from the pit. Although several studies have been conducted on the origin of this groundwater and this site's hydrogeology, its true origins are not well defined. For instance, Jahanshahi and Zare (2017) reported that the Kheirabad salt playa (SP), 13 km north of the mining area, was the main source of the saline groundwater and brines, assuming that the dewatering processes in the Golgohar iron mine (pit no. 1) had formed a cone of depression in groundwater systems around the mine. In such conditions, the natural hydrodynamic balance of saline and fresh water could have been changed, and salt water intruded from the playa into the mine area through faults and fractures. However, using hydrochemical and isotopic evidences, Heidari-Nejad et al. (2017) suggested that there are two aquifers in the mine area that are hydraulically interconnected; an upper alluvial aquifer and a lower hard-rock aquifer. Based on various chemical and isotopic techniques, they proposed that the main source of recharge into the alluvial aquifer was from modern precipitation with deep basin water being the most probable origin of the hard-rock brines. However, current understanding of the origins of the brines in this area does not correlate with various geological and hydrogeological evidence, including the lithological changes of alluvium with the location of springs and seepage faces, sudden and unexpected hydrochemical changes

in the groundwater, and groundwater age dating. Identifying the origin of groundwater is crucial for regulatory, environmental, and economic objectives, such as designing a dewatering system in the mining areas, extraction of some metals from saline groundwater, and assessment of storage/discharge rates of saline water from the aquifers. Therefore, the objectives of this study were to distinguish the origin of groundwater in the Gohar-Zamin mining area, investigate the hydrochemical factors controlling the evolution of groundwater, and provide a comprehensive conceptual model for a complex multi-aquifer system.

Materials and Methods

Geological Framework

The Gohar-Zamin iron mine has an area of $\approx 450 \text{ km}^2$ and is located the main part of the Golgohar metamorphic complex (GMC) in south-central Iran (Fig. 1). This area has become an industrial region (especially with regard to iron and steel production) in recent decades and includes six active iron mines and associated pelletizing-steel industries. Pit no. 3 of the Gohar-Zamin iron ore mine, with a diameter of $\approx 2 \text{ km}$ consisting of 19 benches that range from 1735 to 1450 m above mean sea level (AMSL).

The GMC is located in the structural zone of Sanandaj-Sirjan, the most active tectonic zone of Iran, which has passed through different phases of metamorphism and magmatism (Maknoui Gilani 2019; Soltaninejad et al. 2018). Metamorphic rock belonging to the Precambrian (the Pan-African orogenic episode) and Carboniferous (Hercynian orogenic episode) periods, including disturbed series of mica schist, amphibolite, gneiss, quartzite, and crystalized limestone and marble, form the main lithology of the GMC (Assari 2019; Heidari-Nejad et al. 2017; Maknoui Gilani 2019). The GMC is entirely covered by unconsolidated Quaternary deposits and young terraces. Based on the geotechnical log of 183 exploring boreholes, the maximum and minimum thickness of the alluvial deposits are $\approx 240 \text{ m}$ and 50 m to the west and north of the pit, respectively (Assari 2019).

From the ground surface to benches 13–14, there is a sequence of coarse- and fine-grained strata underlain by a hard-rock formation. The alluvial deposits mainly consist of chert, carbonate, and acidic igneous rock fragments as the weak-cemented coarse-grain strata, which are stratified by mudstone and claystone as the impermeable fine-grain interbed. Most of this study area is occupied by alluvial flatlands with some mountainous areas around. Mountains Bagh-Chubi, Ein-Albaghar, and Chah-Deraz surround the alluvial plains in the north, south, and east, respectively, which are primarily composed of recrystallized limestone, marble, schist, and granite. The Kheir-Abad SP is located

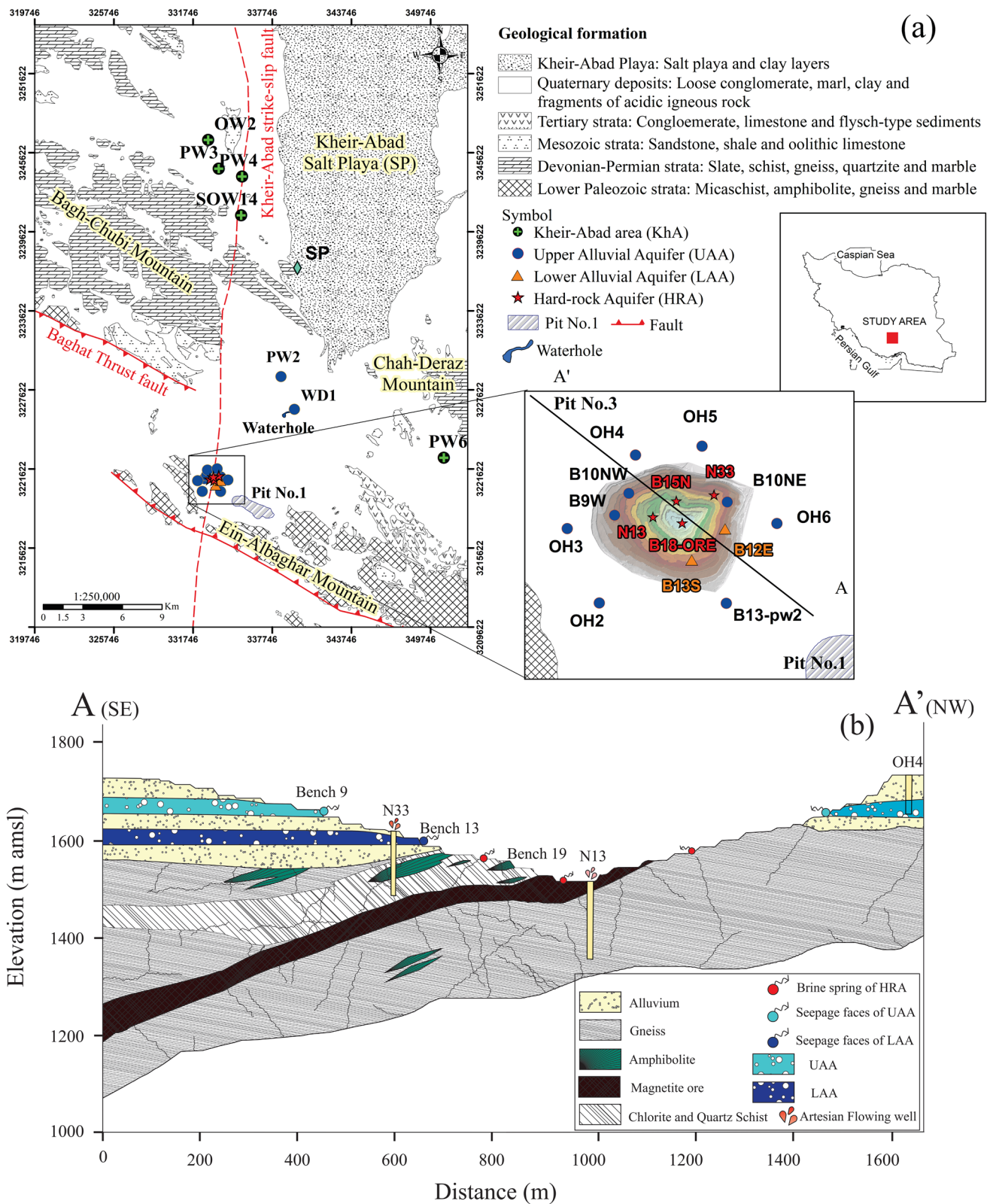


Fig. 1 a Geological map and location of the sampling sites and b generalized cross section A–A'

13 km north of the mines and has been considered a terminus for the accumulation of groundwater and surface water. Hydrodynamically, surface water and regional groundwater in the study area flow toward the playa following the local topography. This basin is a closed inland basin and evaporation is the only output component of accumulated water in the playa.

The study area lies in a semi-arid to arid region with few ephemeral rivers; the mean annual precipitation is ≈ 170 mm, mostly occurring as rainstorms during late winter and early spring (Jahanshahi and Zare 2017). Contrastingly, the average potential evaporation is about $2800 \text{ mm year}^{-1}$ (Maknoui Gilani 2019). The permeable alluvial strata and impermeable fine-grained interbed with a total thickness of ≈ 100 m have formed a complex alluvial aquifer system. The first occurrence of groundwater seeps into the pit at bench 9 in the alluvium (pit no. 3; Fig. 1b). A mudstone interbed has shaped at least two distinct alluvial aquifers: the upper alluvial aquifer (UAA) and the lower alluvial aquifer (LAA). The groundwater elevation of the UAA is about 1,680 m AMSL, and groundwater enters the pit through seepage faces in benches 9, 10, and northwest of 11 with an EC range of $5000\text{--}9000 \mu\text{S cm}^{-1}$. Groundwater from the LAA outcrops at an elevation of 1630 m above MSL with an EC range of $20,000\text{--}30,000 \mu\text{S cm}^{-1}$. The LAA shows less discharge than the UAA, and only appears on the southwestern to eastern sides of benches 12–14 because the lower rock formation slopes north upward (Fig. 1b). It seems that several meters of mudstone prevent the hydraulic interconnection between the UAA and LAA. A silica-cement conglomerate and metasandstone layer 10 m thick is considered to be the bedrock of the LAA. After bench 14, there is a confined hard-rock aquifer (HRA) into the crushed metamorphosed rocks. The HRA's brine discharges into the pit through joints and fractures and have EC values $> 100,000 \mu\text{S cm}^{-1}$.

Evidence, including lithological, hydrodynamic, and hydrochemical evidence, suggests the possible occurrence of a multi-aquifer system in the study area. Permeable coarse-grained layers can be seen in benches 9–10 and 13–14, which are interbedded by impermeable mudstone and claystone. There are several small normal and inverse faults in the coarse-grained layers that terminate in a fine-grained layer (Assari 2019). Hydrodynamic evidence emerges from the seepage faces and springs at benches 9–10 and 13–14 of the pit. The bed layer of this aquifer includes fine-grained layers, and the seepage faces discharge where the coarse- and fine-grained layers contact, whereas there is no evidence of groundwater seepage between these levels (Gharaat et al. 2020). Hydrochemical evidence can be seen in the sudden and unexpected changes in primary properties of groundwater chemistry. The EC values in groundwater of benches 13–14, for example, are over three times the EC values of groundwater in benches 9–10. In the hard-rock brines, this

parameter increases to more than ten times the alluvial groundwater. These sudden changes were also observed in other physicochemical parameters such as TDS, pH, Eh, temperature, major, and minor concentrations (Gharaat et al. 2020).

Groundwater and Surface Water Sampling

Water samples were collected from agricultural wells, a natural waterhole, and geotechnical boreholes. In addition, the piezometers around the mines pits, seepage faces in trenches of the pits, springs in the alluvial and hard-rock aquifers, and a SP were sampled. Methods of sampling and preparations before laboratory analyses were based on the USGS standards (Knapton 1985). A total of 106 samples were collected from 24 sampling stations during six sampling events in January, March, April, May, August, and November of 2019, respectively (Supplemental Table S-1). January and May were considered as dry and wet seasons, respectively, based on the long-period average monthly rainfall of the study area. Because most of the rainfall in the study area occurred from January to May, the sampling had greater temporal resolution at the beginning and a lesser one toward the end of the sampling period. From the total samples, 46 and 24 samples were collected from the upper and lower alluvial aquifers (UAA and LAA), and the hard-rock aquifer (HRA), respectively. Moreover, from the Kheirabad aquifer (KhA), 31 samples were collected from agricultural wells, four samples from a natural waterhole, and one sample from a SP (Table S-1). The location of all the collected water samples is illustrated in Fig. 1a.

In situ parameters such as pH, EC, Eh, and temperature were measured on-site for all the sampling stations using a portable multi-sensor (Hach HQ40D). The accuracy of the multi-sensor for EC, pH, Eh, and temperature was $0.1 \mu\text{S cm}^{-1}$, 0.1, 0.1 mV, and $0.1 \text{ }^\circ\text{C}$, respectively. Before each sampling event, all of the devices and sensors were calibrated based on their manual to ensure the quality of data collected. Furthermore, repetitive control samples from some sampling points (B9W, N13, PW3, and SP), were sent to the laboratory to ensure analytical quality.

Major Ions and Metals Analysis

The water samples were filtered through a $0.45 \mu\text{m}$ Sartorius membrane filter and then stored at $4 \text{ }^\circ\text{C}$ in two acid-washed polyethylene dark bottles, until analysis. One of the bottles was acidified to $\text{pH} < 2$ using concentrated HNO_3 (nitric acid 65%) for Na^+ , potassium (K^+), calcium (Ca^{2+}), magnesium (Mg^{2+}), aluminum (Al^{3+}), barium (Ba^{2+}), strontium (Sr^{2+}), lithium (Li^+), iron (Fe^{3+}), lead (Pb^{2+}), zinc (Zn^{2+}), nickel (Ni^{2+}), mercury (Hg^{2+}), and silver (Ag^+) analyses. The non-acidified bottles were

used for anion analyses (SO_4^{2-} , Cl^- , HCO_3^- , Br^- , F^- , and NO_3^-). The concentration of these ions were analyzed using inductively coupled plasma atomic spectrometry (ICP-AES), using a 930 compact IC Flex instrument with a detection limit of 0.001 mg L^{-1} at the Central Laboratory of Shiraz University. The major anions were analyzed using a 930 Compact IC Flex ion chromatography. In fresh and brackish water samples, the charge balance of the major ions was less than 5%, while brine samples with less than 10% charge balance values were considered acceptable due to dilution processes during analysis (Table 1).

The groundwater salinity in the studied aquifers may be attributed to salinization derived from deep-basin circulation, halite dissolution, evaporation of modern and paleo-water, and brine intrusion from the SP. The specific ionic relationships were suggested by many studies to assess the factors controlling hydrochemical processes and identify the origin of groundwater salinization (Ait Brahim et al. 2015; Belkhirri et al. 2012; Boschetti et al. 2016; Chen et al. 2014). In this study, we used various ionic relationships including Na^+ vs Cl^- , Cl^-/Br^- vs Na^+/Br^- , Ca^{2+} vs SO_4^{2-} , $(\text{Ca}^{2+} + \text{Mg}^{2+})$ vs HCO_3^- , and $(\text{Ca}^{2+} + \text{Mg}^{2+} - \text{SO}_4^{2-} - \text{HCO}_3^-)$ vs $(\text{Na}^+ + \text{K}^+ - \text{Cl}^-)$ to differentiate the origin of salinity.

Sampling and Analysis of the Stable Isotopes: $\delta^2\text{H}$ and $\delta^{18}\text{O}$

Groundwater samples from 19 sites in January and 20 sites in May of 2019 were collected from the piezometers, seepage faces, agricultural wells, and brine springs and filtered into 20 ml dark glass bottles for $\delta^{18}\text{O}$ and $\delta^2\text{H}$ stable isotope analysis. $\delta^{18}\text{O}$ and $\delta^2\text{H}$ were analyzed at Hydroisotop GmbH, Schweitenkirchen, Germany using Los Gatos Research (LGR) DLT-100 laser spectroscopy. All measured isotope ratios were expressed in delta notation with respect to internationally accepted standards. The measurement precisions were $\pm 0.15\text{‰}$ for $\delta^{18}\text{O}$ and $\pm 1.5\text{‰}$ for $\delta^2\text{H}$.

Climate change should be recorded in fossil or paleo-groundwater by the positive correlation between isotopes in precipitation and groundwater. Changing precipitation isotope content and excess deuterium are two common indicators of climate change (Clark and Fritz 2011). Deuterium excess value (d) in arid regions vary depending on humidity during primary evaporation and can be calculated for any precipitation and groundwater sample (Dansgaard 1964):

$$d = \delta^2\text{H} + 8\delta^{18}\text{O} \quad (1)$$

change in paleoclimate is displayed by a shift in the stable isotope content of groundwater and in deuterium excess (Clark and Fritz 2011).

Sampling and Analysis of Radioactive Isotopes: ^3H and $^{14}\text{C}_{\text{DIC}}$

Groundwater samples were collected from piezometers (N33), seepage faces (B12E and B13S), and brine springs (N13 and B9W) in January 2019 for ^3H and $^{14}\text{C}_{\text{DIC}}$ (dissolved inorganic carbon-14) analysis to determine groundwater age. Samples for ^3H and $^{14}\text{C}_{\text{DIC}}$ analysis were taken in 1 L glass bottles, and after $0.45 \mu\text{m}$ filtration, were sealed with parafilm to minimize any contact with air. The radioactive isotopes of ^3H in water and ^{14}C in dissolved inorganic carbon (DIC) were analyzed at the Environmental Isotope Laboratory, University of Waterloo. Tritium results were expressed in the tritium unit (TU) with an analytical precision of ± 0.8 TU. The ^3H concentration in precipitation is about 10 TU nowadays, having fallen from peak values (> 5000 TU) after nuclear bomb tests (Gue et al. 2015; Heidari-Nejad et al. 2017; Mohammadi 2009; Wang and Jiao 2012). Tritium with a half-life of 12.32 years is used to date young groundwater, but it is not suitable for age dating of old waters. ^{14}C with a half-life of 5730 years is often measured to date the groundwater that is less than 50,000 years old. Radiocarbon content was expressed in percent modern carbon (PMC) with an analytical uncertainty of 0.06–0.18 PMC (Gue et al. 2015).

Results

General Hydrochemical Characteristics

The major ion concentrations and physicochemical parameters of the groundwater varied by $< 10\%$ of the average concentration at each sampling point during the six sampling events (Supplemental Table S-1). This indicated a lack of significant temporal differences in the hydrochemical evidence of water samples, especially for the HRA brines, which seemed to be independent of the occurrence of meteoric water (Fig. 2). However, statistical tests were applied to confirm the lack of differences between the temporal analyses. The Kruskal Wallis test was used to investigate the separation or dependence between the results of the six sampling events; the results revealed that there were no significant differences in hydrochemical characteristics of groundwater (Supplemental Table S-2). Consequently, to minimize the uncertainty of the data, the average of the data from the six sampling events was used to identify the origin of groundwater and the mechanism of salinity (Table 1).

Water facies of the different water types were distinguished using the hydrochemistry data plotted on a Piper diagram (Fig. 3). All the groundwater and surface water samples in the study area were Na-Cl water type in a range of salinities from relatively fresh water with a TDS of 1.1 g

Table 1 Analytical data from different water sources in the study site (the data are the average values of six sampling events)

Water sources	Sampling point	TDS (g l ⁻¹)	pH	Na ⁺ mg l ⁻¹	K ⁺	Ca ²⁺	Mg ²⁺	Cl ⁻	SO ₄ ²⁻	HCO ₃ ⁻	Br ⁻	Li ⁺	Charge balance (%)	Cl ⁻ /HCO ₃ ⁻ weight ratio	Cl ⁻ /SO ₄ ²⁻ weight ratio	Na ⁺ /Cl ⁻ molar ratio	Br ⁻ /Cl ⁻ molar ratio
HRA	N13	145.4	6.7	38,551.0	409.3	17,874.4	2052.4	85,222.3	2110.6	35.2	47.3	21.7	5.8	2415.6	40.3	0.6976	2.5E-04
	B18-ORE	148.8	6.7	50,491.3	500.0	21347.4	3167.8	106,483.0	3089.5	34.6	57.3	29.1	7.1	3,073.1	34.4	0.731	2.4E-04
	Mixed P.W ^a	101.3	6.7	24,085.1	202.4	10,195.8	1418.7	65,061.5	1258.5	50.4	41.1	15.9	5.2	1290.9	51.7	0.5711	2.8E-04
	N33	71.7	6.9	20,181.9	191.1	9517.0	1238.6	42,648.4	1697.1	47.2	39.6	18.2	8.2	902.6	25.1	0.7298	4.1E-04
	B15N	81.9	6.8	26,947.6	248.5	11,956.9	978.0	49,239.5	1305.5	49.1	32.3	19.9	9.4	1002.0	37.7	0.8438	2.9E-04
	B13S	20.9	7.1	5808.0	44.6	2419.9	384.0	11,274.3	961.5	90.3	10.5	5.0	8.9	124.8	11.7	0.7943	4.2E-04
	B12E	17.5	7.3	4596.2	37.3	2078.6	438.9	9728.3	1008.2	117.6	9.0	3.6	6.8	82.7	9.6	0.7285	4.1E-04
	B9W	4.3	7.7	907.2	10.0	432.1	144.1	1624.5	707.0	129.1	1.5	0.3	6	12.5	2.3	0.9703	4.2E-04
	B10NE	6.4	7.6	1673.7	13.6	571.5	130.1	2891.6	878.8	134.8	2.2	1.3	7	21.4	3.2	0.9539	3.4E-04
	B10NW	7.2	7.6	1075.1	14.1	628.2	208.4	3,105.5	701.0	115.5	2.8	0.4	1.7	26.8	4.4	0.5909	4.1E-04
LAA	OH2	3.3	7.8	538.6	4.8	261.5	104.2	1359.8	639.6	148.0	1.2	0.2	3.8	9.1	2.1	0.7411	4.1E-04
	OH3	5.7	7.7	1054.6	17.9	577.9	186.3	2080.4	901.6	122.8	1.5	0.3	6.2	16.9	2.3	0.8669	3.2E-04
	OH4	3.1	7.8	706.2	6.5	323.3	77.2	1193.2	595.5	138.6	1.2	0.3	6.4	8.6	2.0	1.0612	4.5E-04
	OH5	3.2	7.8	709.6	5.4	280.4	100.3	1338.8	769.8	126.0	1.1	0.2	2.1	10.6	1.7	0.9497	3.7E-04
	OH6	8.8	7.9	1431.6	14.7	560.5	169.0	3736.4	877.5	119.7	3.3	0.7	6.8	31.2	4.2	0.6382	3.9E-04
	B13-pw2	7.5	8.4	1764.3	14.9	722.6	211.8	3268.3	918.2	139.6	3.0	1.0	8.7	23.4	3.5	0.8866	4.1E-04
	WD1	14.2	7.8	2762.2	21.8	1416.8	230.2	6200.7	824.0	129.1	4.3	1.3	5.2	48.0	11.3	0.7158	3.1E-04
	PW2	3.7	7.8	1328.6	13.6	219.6	50.0	1905.0	167.8	290.8	0.9	0.4	1.6	6.5	7.5	1.2069	2.7E-04
	PW3	1.4	7.6	296.3	3.4	105.2	21.1	483.7	170.7	217.3	0.5	0.1	1.9	2.2	2.8	0.945	4.8E-04
	PW4	7.2	7.4	1920.7	21.1	539.3	152.6	3,389.3	337.4	185.8	1.5	0.7	7.8	18.2	10.0	0.874	2.1E-04
Kha	PW6	1.1	7.7	264.9	4.9	105.0	37.5	283.2	326.5	201.6	0.7	0.1	9.9	1.4	0.8	1.4416	1.1E-03
	SOW14	1.1	7.8	287.9	8.5	107.1	21.4	414.1	57.7	221.5	0.3	0.1	2.7	1.8	7.1	1.0728	3.3E-04
	OW2	1.1	8.0	265.1	2.8	74.8	24.0	352.7	228.0	217.3	0.3	0.1	3.1	1.6	1.5	1.1589	3.8E-04
	Salt playa	321.1	7.0	147,976.0	595.0	19,384.0	5,961.0	230,555.0	8392.0	88.2	2,30.0	19.0	3.1	2614.0	27.4	0.9899	4.4E-06

^aMixed PW (Mixed pumping water) is a mixture of hard-rock and alluvial water that accumulates on bottom of the pit that is then pumped to an evaporation pond

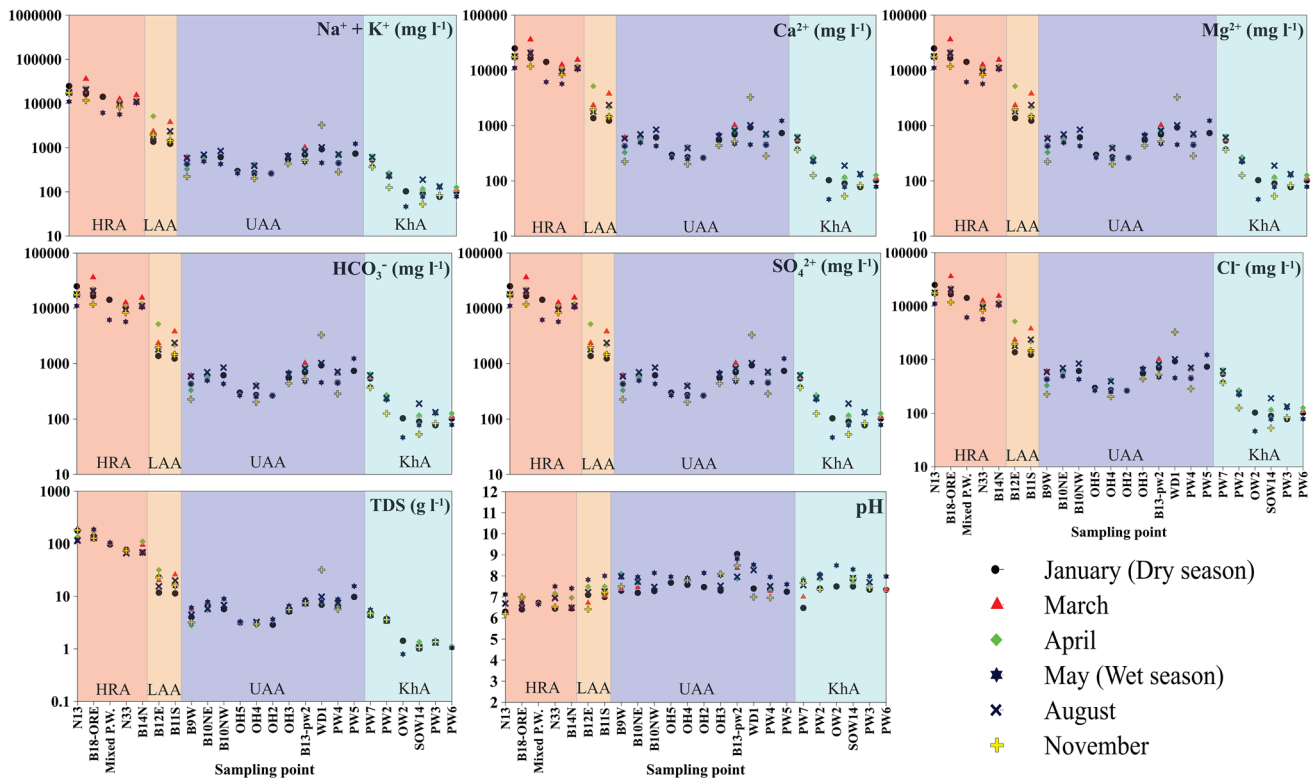


Fig. 2 Variation of the major ions and physicochemical parameters in groundwater during six sampling periods

L^{-1} in the agricultural wells of KhA to hypersaline brines in SP with a TDS of 321.1 g L^{-1} . The maximum salinity at the mining area was found in the HRA brines that outcropped through cracks and joint sets of the hard-rock formation.

The $\text{Cl}^-/\text{HCO}_3^{2-}$ weight ratios ranged from 1.6 to 2.2 at KhA (except for PW4), 6.6 to 31.2 at UAA (except for WD1), 82.7 to 124.9 at LAA, and 902.6 to 3073.1 at HRA (Table 1). Due to the overexploitation of groundwater in the Kheirabad aquifer (KhA), agricultural wells such as PW4 have been affected by salt-water intrusion from the SP. WD1 is also a natural waterhole where evaporation plays an important role in the excess concentration of Cl^- in the ratio $\text{Cl}^-/\text{HCO}_3^-$. Furthermore, $\text{Cl}^-/\text{SO}_4^{2-}$ weight ratios likewise ranged from 0.9 to 7.1 (except for PW4) in KhA, from 1.7 to 7.5 (except for WD1) in UAA, from 9.6 to 11.7 in LAA, and from 25.1 to 51.7 in HRA. The $\text{Cl}^-/\text{HCO}_3^-$ and $\text{Cl}^-/\text{SO}_4^{2-}$ ratios in SP were about 2614 and 27.5, respectively (Table 1).

Na^+ and Cl^- were the dominant major cations and anions in most of the groundwater samples (Table 1), where a stronger linear relationship between Na^+ and Cl^- ($R^2 > 0.9$) suggested a common providing source(s) (Fig. 4). As illustrated in Fig. 4, the concentration of the major elements of the aquifers are drastically contrasting. Consequently, hydrochemical properties of groundwater have distinctly changed between UAA, LAA, HRA, and KhA. This indicated a lack

of hydraulic relationship between the aquifers where mixing processes were not observed. Furthermore, the low bicarbonate contents in UAA, LAA, and especially HRA (relative to KhA) can be primary evidence attributed to the fact that the aquifers lack an active connection to the rapid circulation of meteoric water (Table 1).

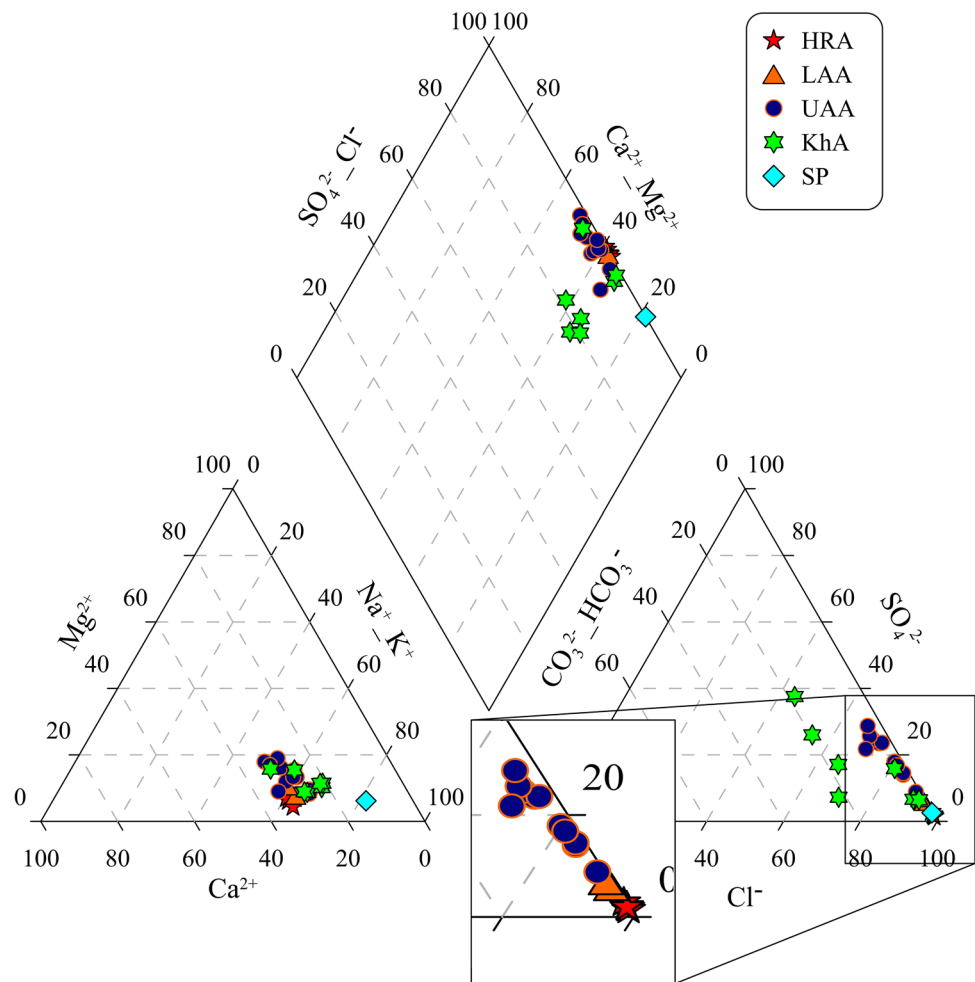
Ionic Relationships

Halite Dissolution Origin

Ionic ratios of conservative and quasi-conservative ions such as Na^+/Cl^- and Br^-/Cl^- are reliable ways to identify the origin of groundwater salinization (Eggenkamp et al. 2019). When Na^+/Cl^- molar ratios were > 1 and Br^-/Cl^- weight ratios were $\approx 4 \times 10^{-4}$, the origin of salinization was considered to be halite-solution brine. Conversely, the brine water was considered to be deep-basin brine or seawater intrusion when the Na^+/Cl^- molar ratios were less than 0.86 (seawater value) and the Br^-/Cl^- weight ratios $> 25 \times 10^{-4}$ (Bagheri et al. 2014a, b).

Na^+ and Br^-/Cl^- ratios vs Cl^- are plotted in Figs. 4 and 5. Notably, the ratios of Na^+/Cl^- and Br^-/Cl^- in most water samples exhibited values expected for those of halite-solution origin. Na^+/Cl^- ratios greater than 1:1 in KhA indicate a relative increase of Na^+ ions compared to Cl^- (Fig. 4).

Fig. 3 Piper diagram for the chemical composition of groundwater in the aquifers. The zoomed rectangle is the chemical composition of water samples in the mining area



Moreover, the Na^+/Cl^- molar ratio is constantly greater than 0.95 in fresh meteoric water (Khaska et al. 2013). Therefore, KhA is perhaps recharged by local fresh meteoric water. The groundwater analysis of HRA demonstrated that Na^+/Cl^- molar ratios were slightly less than unit values in the range of 0.57 to 0.84 (Fig. 4 and Table 1), indicating rock-water interactions and reverse cation exchange, as explained above.

The molar relationship of Na^+/Br^- vs Cl^-/Br^- is a practical way to identify two different sources of salinization: halite dissolution and evaporation of water (Fig. 6). Particularly, Br^- is considered more conservative than both Cl^- and Na^+ (Bagheri et al. 2014a, b; Eggenkamp et al. 2019). Thus, when water evaporates, Br^- scarcely precipitates into the solid evaporites. As the evaporation increases, the Na^+/Br^- and Cl^-/Br^- ratios decrease, whereas with halite dissolution, the concentrations of Cl^- and Na^+ increase by equimolar amounts relative to Br^- content (Bagheri et al. 2014a, b). The Na^+/Br^- and Cl^-/Br^- molar ratios of all measured groundwater and surface water samples resided in the expected ranges for the halite dissolution trend line (Fig. 6). The evaporation processes did not affect the infiltrated

meteoric water because halite dissolution is the dominant force for groundwater salinization.

The results from these ratio analyses disagreed with the assumption of possible sources of evaporation and/or deep-basin saline waters as the main source of groundwater salinity. However, many groundwater samples in HRA and LAA reflect significant excess amounts of Ca^{2+} and Mg^{2+} and deficient Na^+ levels. The enrichment or depletion of Ca^{2+} , Mg^{2+} , and Na^+ is perhaps caused by precipitation or dissolution of carbonate and sulfate minerals and/or cation exchange in the aquifer (Baudron et al. 2013; Gue et al. 2015; Qiao et al. 2019; Scheiber et al. 2015). In the following, these possible processes are separately evaluated.

Gypsum and Carbonate Dissolution

The $\text{Ca}^{2+}/\text{SO}_4^{2-}$ ratio can be used as an indicator of precipitation or dissolution of the sulfate minerals such as gypsum and anhydrite. The solubility of gypsum is higher than that of anhydrite, especially in the presence of halite and mutual ions (Gue et al. 2015). When the ratio $(\text{Ca}^{2+} + \text{Mg}^{2+})/\text{HCO}_3^-$ has a value of $\approx 1/2$, it is concluded

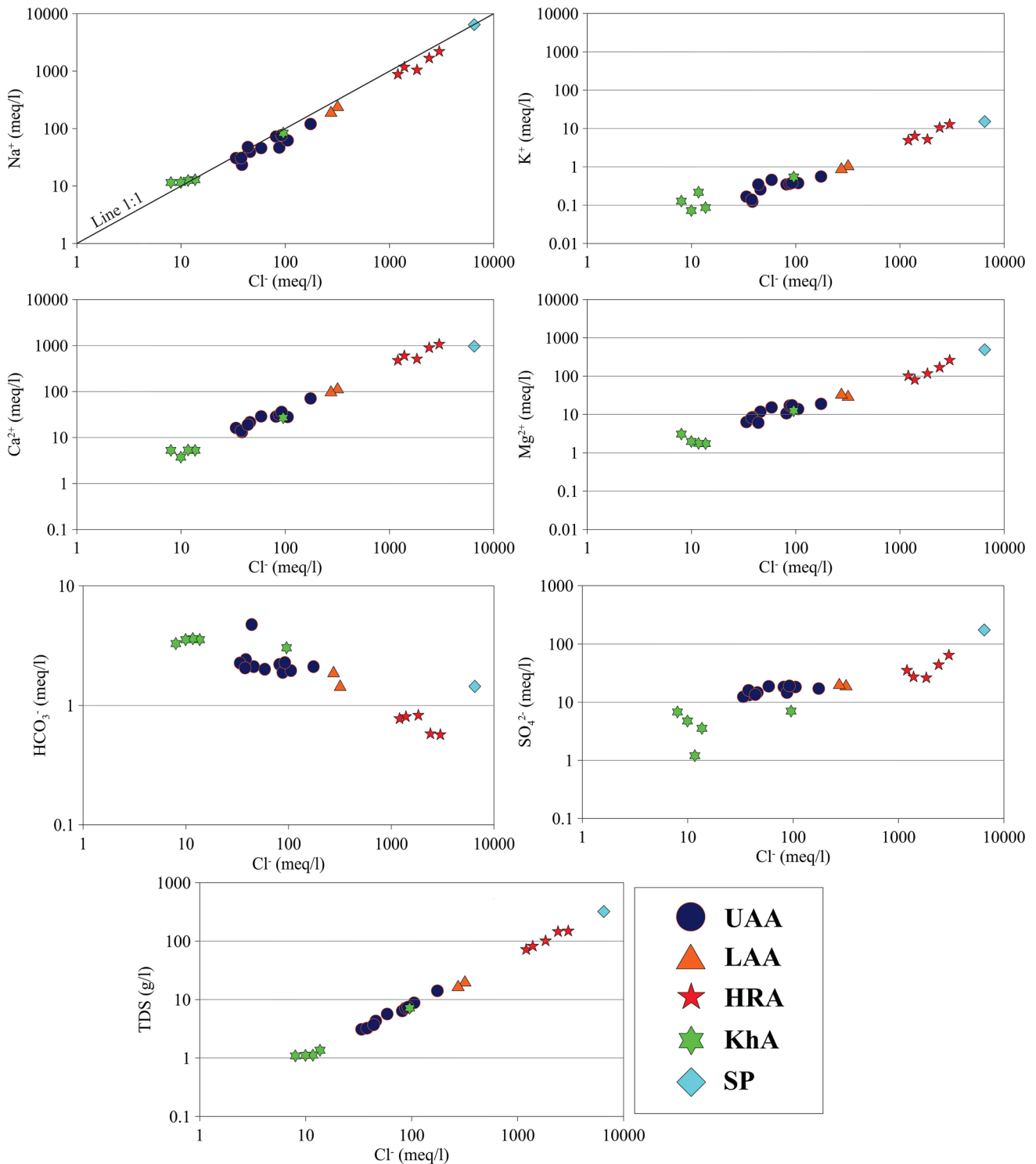


Fig. 4 Relationships between 6-step average concentrations of the major cations and anions and TDS versus chloride

that the main Ca^{2+} source in groundwater is calcite dissolution. However, when this ratio is $\geq 1/4$, the groundwater has probably dissolved a significant amount of dolomite (Argamasilla et al. 2017).

The measured concentrations of Ca^{2+} and SO_4^{2-} are presented in Fig. 7 and are compared with the theoretical dissolution lines of sulfate minerals. The results indicate that sulfate mineral dissolution is the major source Ca^{2+} and Mg^{2+}

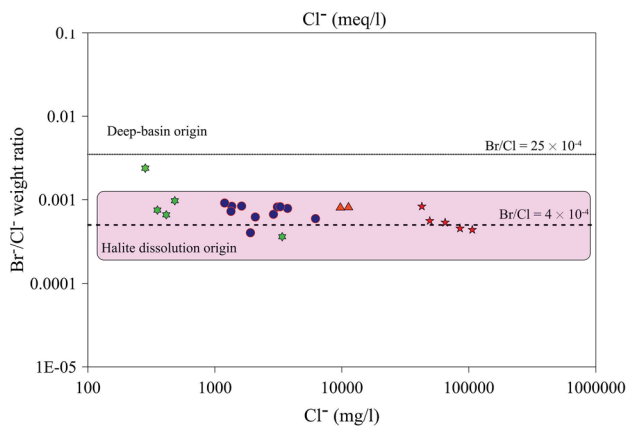


Fig. 5 Br⁻ vs Cl⁻ for groundwater samples of KhA, UAA, LAA, HRA, and SP. Dashed line is the theoretical line of halite dissolution

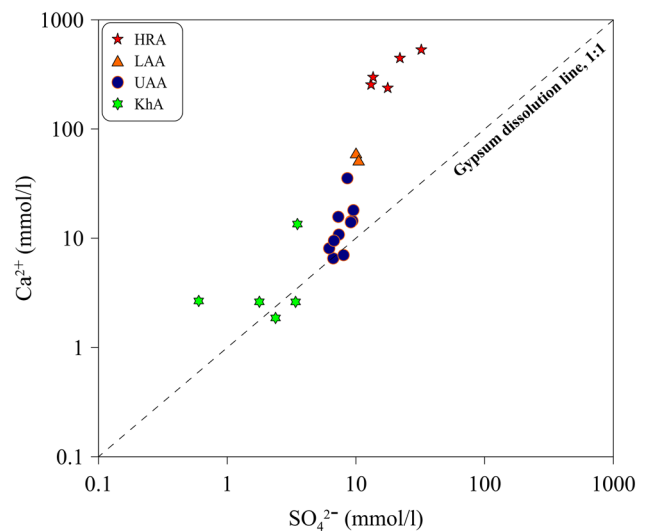


Fig. 7 The concentrations of SO₄²⁻ versus Ca²⁺ measured in water samples. The ratios below the drawn lines represent the stoichiometric relationships between paired solutes. Dashed line refers to dissolution of sulfate minerals (gypsum and anhydrite)

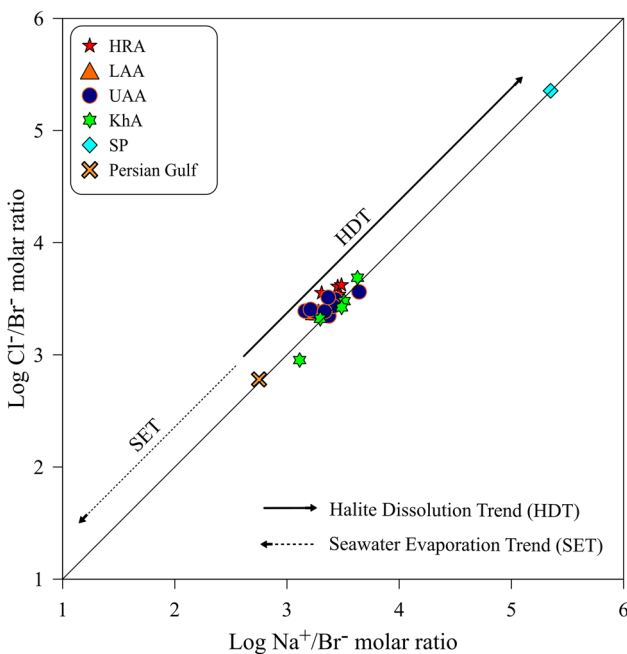


Fig. 6 The relationship between Cl⁻/Br⁻ and Na⁺/Br⁻ ratios of the groundwater samples. All the water samples are aligned along the Halite Dissolution Trend (HDT). Seawater evaporation trend (SET) is extensively used to analyze the origin of salinity in the sedimentary basins (Bagheri et al. 2014a, b)

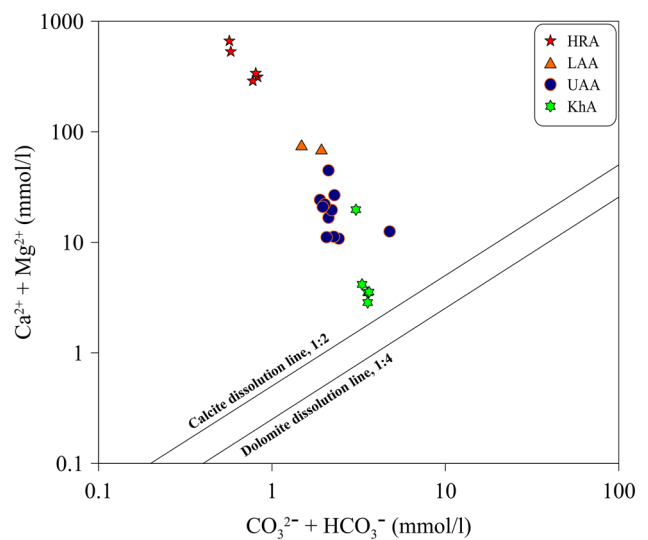


Fig. 8 Characteristic ionic relationships of Ca²⁺ and Mg²⁺ versus HCO₃⁻ and CO₃²⁻ in the groundwater samples. Dissolution of dolomite was not observed in any groundwater samples, and only the groundwater samples near the Devonian-Permian marbles (Bagh-Chubi Mountains) dissolved carbonate minerals

in the KhA and UAA, whereas the excess Ca²⁺ + Mg²⁺ in HRA and LAA, in addition to sulfate dissolution, are due to other chemical processes such as rock-water interaction (Fig. 7).

The carbonate sequence in the study area belongs to the Paleozoic and Mesozoic metamorphic rock series and outcrop as marble and metamorphosed limestone south and north of the KhA (Fig. 1). The relationships of the dissolved Ca²⁺ and Mg²⁺ vs HCO₃ are illustrated in Fig. 8 and

compared with the theoretical dissolution line of calcite and dolomite. As shown in Fig. 8, only water samples of KhA have (Ca²⁺ + Mg²⁺)/HCO₃⁻ molar ratios close to 1/2, whereas this ratio in LAA and especially HRA show a remarkable enrichment of Ca²⁺ and Mg²⁺. This suggests that in addition to halite dissolution, carbonate and sulfate mineral dissolution contribute to the main chemistry of waters in the KhA. However, the excess concentration of Ca²⁺ and Mg²⁺

in groundwater of LAA and HRA cannot be due to carbonate and sulfate mineral dissolution alone; reverse cation exchange likely occurred.

Cation Exchange

The ratios of $(\text{Ca}^{2+} + \text{Mg}^{2+} - \text{SO}_4^{2-} - \text{HCO}_3^-)$ and $(\text{Na}^+ + \text{K}^+ - \text{Cl}^-)$ are usually used to evaluate the role of cation exchange occurring in an aquifer (Montcoudiol et al. 2015; Qiao et al. 2019; Yuan et al. 2017). The contents of Na^+ , K^+ , and Cl^- are almost equal if only halite dissolution has occurred. The moles of Ca^{2+} and/or Mg^{2+} deriving from the dissolution of carbonate and sulfate minerals are equal to the sum of the moles of SO_4^{2-} and HCO_3^- . Using the scatterplot of $\text{Na}^+ + \text{K}^+ - \text{Cl}^-$ vs $\text{Ca}^{2+} + \text{Mg}^{2+} - \text{HCO}_3^- - \text{SO}_4^{2-}$, the x -axis represents the excess concentration of Na^+ and K^+ from sources other than halite dissolution or evaporation; meanwhile, the y -axis represents the Ca^{2+} and/or Mg^{2+} derived from processes other than carbonate or gypsum dissolution. Therefore, if the dissolved major elements were derived from the dissolution of halite, carbonate, and sulfate minerals, then all the data should plot near the origin of the coordinates (0, 0) of the graph (Argamasilla et al. 2017; Huang et al. 2013; Owen and Cox 2015).

As expected, the groundwater samples of HRA and LAA showed excess amounts of $\text{Ca}^{2+} + \text{Mg}^{2+}$ (Fig. 9). Ca^{2+} and Na^+ display opposite behaviors. Enrichment of Ca^{2+} and Mg^{2+} is coinciding with the depletion of Na^+ concentration in groundwater of HRA and LAA and can only be explained by reverse cation exchange (Fig. 9). The exchange of Ca^{2+} (and/or Mg^{2+}) and Na^+ may have occurred in HRA

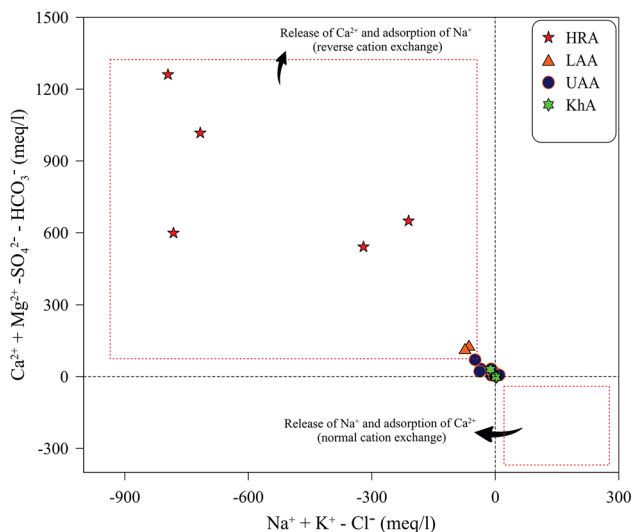


Fig. 9 The binary graph of the major ions to interpret the hydrochemical rock-water interactions, mixing of water, and processes such as dissolution of halite, carbonate, and sulfate minerals. In the coordinate origin (0, 0) only halite, calcite and gypsum are dissolved

to balance the excess concentration of Na^+ in Na^+ -rich primary recharged groundwater. Previous studies on heavy metals and pollution levels of groundwater in the mining area have shown significant amounts of heavy metals and major and minor elements have transferred from the solid phase (metamorphic rocks) to the hard-rock brines by water–rock reactions (Jahanshahi and Zare 2015).

Stable Isotope Signatures

The mean isotope compositions of groundwater and surface water samples during dry and wet seasons are summarized in Table 2 and illustrated in Fig. 10. The local meteoric water line (LMWL) for the study area was measured and projected by Jahanshahi and Zare (2017) as $\delta^2\text{H} = 7.12$, $\delta^{18}\text{O} + 15.92$ and is compared with the global meteoric water line (GMWL) (dashed line in Fig. 10). The SP had $\delta^{18}\text{O}$ and $\delta^2\text{H}$ of -3.86‰ and -47.2‰ and was significantly depleted when compared to the LMWL of the Sirjan area and the groundwater samples (Fig. 10). This is due to the salinization effects on ion hydration. The effects of solutes are critical in the measurement of stable isotopes in brines whereas in supersaturated waters, ion hydration causes a depletion of $\delta^{18}\text{O}$ and $\delta^2\text{H}$ because the isotope activity decreases with increasing salinity (Clark and Fritz 2011).

All the groundwater samples had stable isotope values below the LMWL; the samples from KhA were the closest to LMWL (Fig. 10a). The ^{18}O and ^2H have conservative compositions and cannot be greatly affected by precipitation and dissolution in a short time. Therefore, the evident differences of $\delta^{18}\text{O}$ and $\delta^2\text{H}$ between the UAA, LAA, and HRA aquifers and the LMWL suggest that the origin(s) of groundwater in the aquifers has/have no significant connection to the modern circulation of the meteoric water. The isotopic composition of groundwater is generally controlled by meteorological processes (Clark and Fritz 2011). However, different natural processes can cause the stable isotope contents in reservoir waters to deviate from the LMWL equilibrium values (Fig. 10b, modified by D'Amore and Panichi 1985). Equilibrium exchange of the ^{18}O in groundwater with aquifer materials may produce ^{18}O enriched groundwater (Dor et al. 2011; Karolytė et al. 2017). In some cases, deep groundwaters may be enriched in ^{18}O relative to the GMWL, while ^2H values remain unchanged due to isotope exchange with the minerals of the host materials (Clark and Fritz 2011). Interestingly, $\delta^{18}\text{O}$ contents in UAA, LAA, and HRA were progressively enriched with almost the same $\delta^2\text{H}$ relative to LMWL (Fig. 10a). This can be attributed to rock-water interactions in groundwater with high residence times because ^2H is relatively more conservative, while ^{18}O enters chemical reactions more than ^2H . One sample in KhA and two samples in UAA were collected from surface water bodies (topographic depression) and were affected by evaporation

Table 2 Mean values of stable and radioactive isotopic parameters analyzed in groundwater and surface water samples

Water sources	Samples	$\delta^{18}\text{O}$ (‰)	$\delta^2\text{H}$ (‰)	Deuterium excess (‰)	^3H (TU)	^{14}C (pmc)	Apparent age (ybp)
UAA	B9W	-5.675	-36.95	8.45	<0.8	46.22	6200
	OH3	-5.145	-35.55	5.61			
	OH4	-6.01	-37.45	10.63			
	B10NE	-5.3	-36.15	6.25	<0.8		
	B13-pw2	-5.385	-36.7	6.38			
	WD1	-4.18	-27.8	5.64			
	PW2	-4.44	-27.1	10.42			
LAA	B13S	-4.99	-34.6	5.32		9.725	18,720
	B12E	-4.74	-36	5.12	<0.8	11.28	17,532
HRA	B15N	-3.465	-35.85	-0.13	<0.8		
	N33	-3.38	-36.6	-1.56		3.257	27,508
	N13	-3.11	-34.75	-9.87		3.214	27,616
KhA	B18-ORE	-2.645	-33.3	-12.14			
	PW3	-6.43	-34.6	14.04			
	PW4	-6.005	-32.7	12.67			
	PW6	-6.475	-34.95	14.05			
	SOW14	-6.68	-33.75	16.89			
Salt playa	OW2	-6.615	-34.95	15.17			
	SP	-3.86	-47.2	-16.32			

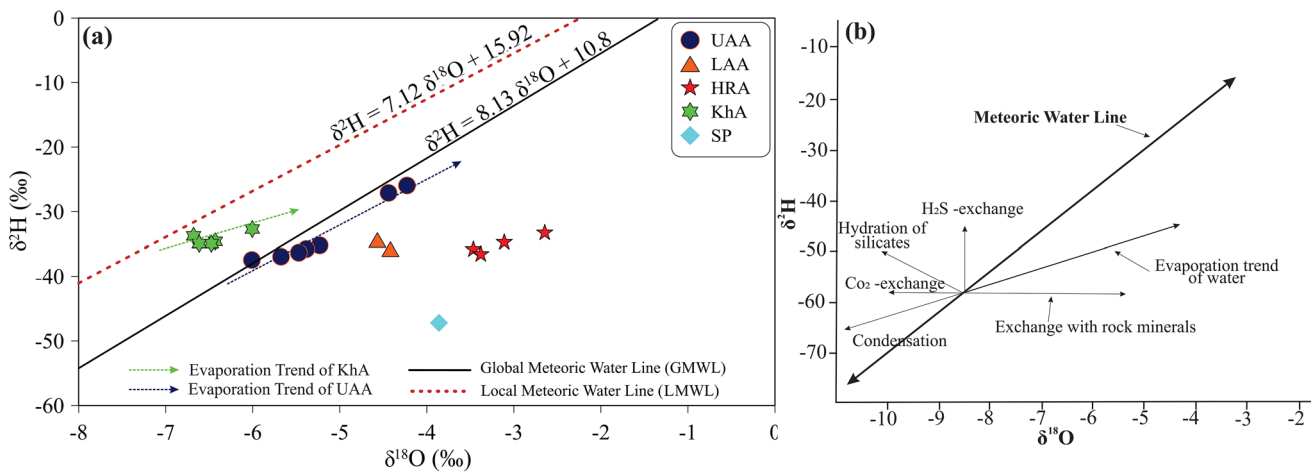


Fig. 10 **a** Stable isotope compositions ($\delta^2\text{H}$ and $\delta^{18}\text{O}$) of the groundwater samples, shown relative to the Global Meteoric Water Line (GMWL) and Local Meteoric Water Line (LMWL) of Sirjan. **b** Pro-

cesses which may affect $\delta^{18}\text{O}$ and $\delta^2\text{H}$ values of water after its infiltration (Clark and Fritz 2011; Karolytė et al. 2017; Pang et al. 2017)

throughout the year. These samples are isotopically enriched and separated from their aquifer types. The evaporation trends of these two shallow aquifers were drawn using the deviation of these samples from the average isotopic contents and indicate that the isotopic enrichment of the deeper aquifers was not due to evaporation in the shallower aquifers (from KhA → UAA → LAA → HRA) (Fig. 10a). Furthermore, the deuterium excess in the groundwater samples of the alluvial aquifers (UAA and LAA) were positive, in the

range of 5.12 to 10.63‰, while the values converged negatively in HRA from -0.13 to -12.14‰ (Table 2). Accordingly, this illustrates the lack of hydraulic interconnection between UAA, LAA, and HRA; the groundwaters in these aquifers are derived from different sources.

$\delta^2\text{H}$ is an approximate conservative parameter in the sedimentary aquifer systems which can be compared with other conservative elements (e.g. Cl^-) to evaluate the origin of groundwater salinity (Bagheri et al. 2014a, b). If evaporation

of groundwater is the central factor for groundwater salinization, the $\delta^2\text{H}$ and Cl^- should be well-correlated (Clark and Fritz 2011; Jahanshahi and Zare 2017). The results of $\delta^2\text{H}$ vs Cl^- showed that increasing salinity in groundwater is associated with constant concentrations of $\delta^2\text{H}$, which highlights evaporite dissolution, especially halite (Fig. 11).

^3H and $^{14}\text{C}_{\text{DIC}}$ Evidence

The ^3H level in all four groundwater samples was below the detection limit of 0.8 TU (Table 2), demonstrating that groundwater at the mining area, even in the youngest aquifer (UAA), was recharged prior to the thermonuclear bomb tests in the 1950s and 1960s (Clark and Fritz

2011). Interestingly, from the measured ^{14}C , the ages of water samples were 6200 ybp (years before present) for the UAA, 18,000 ybp for the LAA, and 27,500 ybp for the HRA (Table 2). The relative apparent ages calculated from ^{14}C agree with the hydrochemical data and isotopic evidence, confirming that UAA, LAA, and HRA have distinctive origins in an unconnected multi-aquifer system (Fig. 12). As shown in Fig. 12, the concentration of Cl^- , coincident with increasing groundwater age, increased significantly in the deeper aquifers (HRA and LAA). Sudden changes in the groundwater age and content of the conservative elements are evidence for the different origins of groundwater. The residence time of groundwater in HRA and LAA was long enough to allow hydrochemical processes such as cation exchange to occur.

Fig. 11 Relation between $\delta^2\text{H}$ and Cl^- concentrations in the groundwater and surface water samples

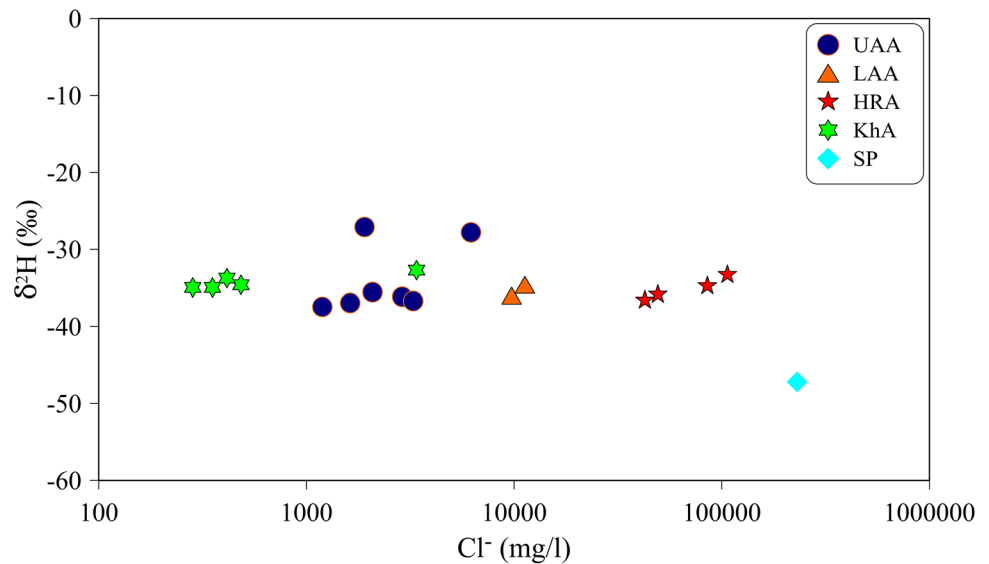
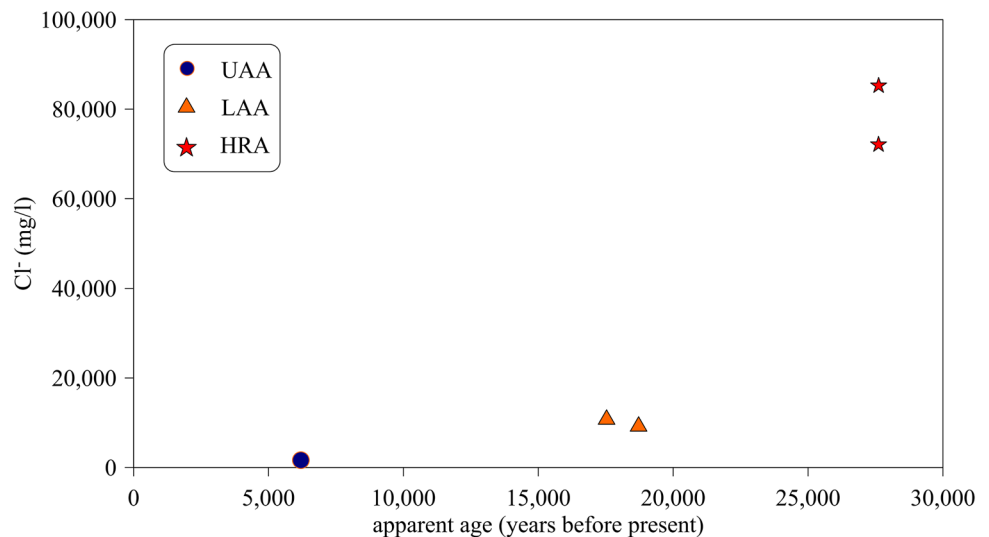


Fig. 12 Measured carbon-14 activity of dissolved inorganic carbon in groundwater samples of the mining area



Discussion

Sources of Groundwater Salinity

The saline groundwater conditions in many arid regions are the result of water evaporation and/or dissolution of evaporated deposits (Abirifard et al. 2017; Kouchekezadeh and Zarei 2017; Nekouei et al. 2016; Zarei et al. 2014). However, research by Su et al. (2020) suggested that groundwater pumping for various uses in arid regions can accelerate water–rock interactions and trigger recharge from saline water, increasing the groundwater salinity in an aquifer. The potential processes causing the salinity in groundwater of the Gohar-Zamin mining area can be attributed to halite dissolution, evaporation of water, brine water intrusion from the SP, and water–rock interactions. The hydrogeology, stratigraphy, structural geology, hydrochemical evidence, and isotope composition help us to better understand the origin of groundwater salinization.

As shown in Table 3, halite dissolution is likely the main origin of groundwater salinity in all water sources in the studied area. In addition to the dissolution of halite in KhA samples, evidence of calcite and gypsum dissolution was also observed; this was expected in the presence of the Ca²⁺-rich marble and schist strata. The high HCO₃⁻ concentrations in the KhA groundwater samples, compared to the rest of the studied aquifers, indicated a hydraulic connection between the KhA groundwater and local meteoric water, which was also supported by the stable isotope analyses.

Based on the specific ionic relationships of the conservative elements, the origin of salinity in the UAA, LAA,

and HRA was attributed to dissolution of halite. In addition, reverse cation exchange has also occurred in LAA and especially HRA due to the long residence time of the Na⁺-rich groundwater, which changes the water chemistry (Table 3). Cation exchange did not occur in the UAA, possibly due to the shorter residence time there (6200 ybp), alkaline earth-poor alluvium, and low Na⁺ content in the groundwater. In addition, no intrusion of brine water was observed from the SP and the evaporation process did not affect the infiltrated paleo-waters formed in the UAA, LAA, and HRA.

Besides the results of this study, the spatial and temporal distributions of 13 metals (Al, As, Co, Li, Mn, Mo, Ni, Pb, Rb, Se, Si, Sr, and Zn) have been evaluated in the Gohar-Zamin mining area by Gharaat et al. 2020. The results showed that with a similar trend of TDS and the major ions, the concentrations of these metals generally decrease (HRA > SP > LAA > UAA > KhA; see Fig. 4 in Gharaat et al. 2020). They concluded that the main source of these metals had a geogenic and lithostratigraphic origin, so temporal changes had no effect on the variations. Therefore, different groundwater origins may explain the varied metal concentrations in the studied aquifers.

Origin of the Groundwater

As reported in previous studies (Assari 2019; Gharaat et al. 2020; Heidari-Nejad et al. 2017; Jahanshahi and Zare 2017) and in greater detail in the present study, there are three separate aquifers in this multi-aquifer system where water flows into the mines from both alluvial and fractured aquifers. The hydrochemical evidence, isotopic properties, and age dating of the groundwater in the studied aquifers

Table 3 Summary of the possible origins of the studied aquifers based on different diagnostic methods

Methods	Aquifers			
	HRA	LAA	UAA	KhA
Ionic ratios	✓: HD, RWI ×: CD, SD, DB, EW	✓: HD, RWI ×: CD, SD, DB, EW	✓: HD, SD ×: CD, DB, EW, RWI	✓: HD, CD, SD, RWI ×: DB, EW
δ ¹⁸ O vs δ ² H	✓: HD ×: BI, EW	✓: HD ×: BI, EW	✓: HD ×: BI, EW	✓: HD, a few EW ×: BI
Age dating	✓: RWI ×: BI	✓: RWI ×: BI	✓: – ×: BI	✓: N ×: N
Lithostratigraphy and historical geology	✓: HD, RWI ×: DB, BI	✓: HD, RWI ×: DB, BI	✓: HD, SD ×: DB, BI	✓: HD, CD, SD ×: DB, BI
Modern and paleo-hydrogeology	✓: HD, RWI ×: DB, BI	✓: HD, RWI ×: DB, BI	✓: HD, ×: DB, BI	✓: HD, CD, SD, RWI ×: DB, BI
The suggested origin of salinity	HD and RWI	HD and RWI	HD and SD	HD, CD and SD

✓ and × signs are confirmation and decline of the specific sources of salinity in each aquifer, respectively. All of the possible origins of groundwater salinization in the studied aquifers are considered as:

HD halite dissolution, CD carbonate mineral dissolution, SD sulfate mineral dissolution, DB deep-basin brines, BI brine water intrusion, EW evaporation of modern and/or paleo-water, and RWI rock-water interactions (especially ion exchange). N means NO data

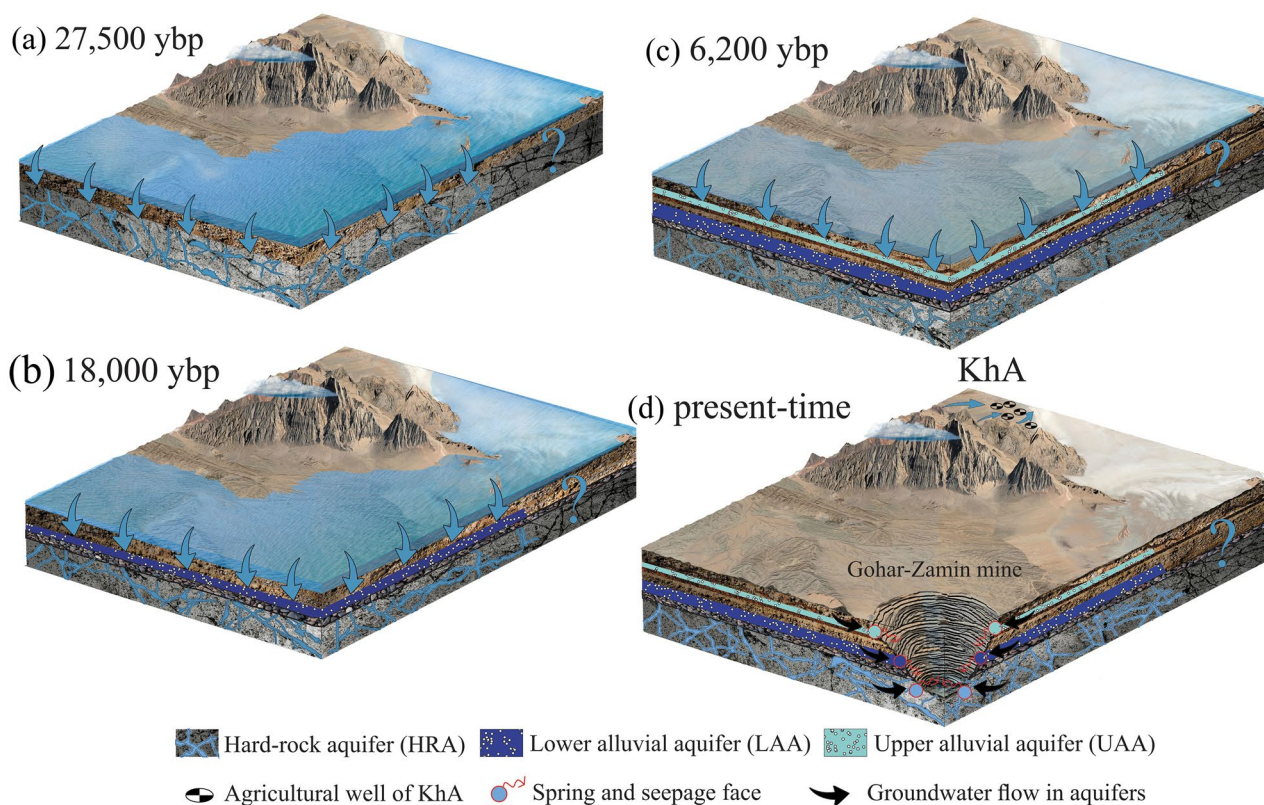


Fig. 13 A conceptual model of groundwater origin in a multi-aquifer system: **a** 27,500 ybp-period that formed HRA with an average EC of $150,000 \mu\text{S cm}^{-1}$, **b** 18,000 ybp-period that formed LAA with an

average EC of $25,000 \mu\text{S cm}^{-1}$, and **c** 6200 ybp-period that formed UAA with an average of EC of $6000 \mu\text{S cm}^{-1}$

allows for a schematic conceptual model of the aquifers' origin (Fig. 13). In this Figure, 3D block diagrams of different hydrogeological environments are presented in three paleo-periods at 6200, 18,000, and 27,500 ybp. The following evidence highlights that in the KhA area, local meteoric rainwater infiltrates into the ground and is mineralized by calcite, gypsum, and halite dissolution:

- The hydraulic gradient in KhA is from the Bagh-Chubi Mountains to SP (Fig. 1 and the arrow signs in Fig. 13d).
- The groundwater of KhA is of the Na–Ca–Cl type (Fig. 3).
- The groundwater samples of KhA are generally less mineralized and their composition is close to that of rainwater (Jahanshahi and Zare 2017).
- The Ca^{2+} , Mg^{2+} , and SO_4^{2-} concentrations at KhA are near the theoretical line of calcite (Fig. 8) and the dissolution line of gypsum (Fig. 7).
- The isotope compositions of the groundwater samples from KhA are near the LMWL (Fig. 10).

However, the following considerations suggest that the UAA, LAA, and HRA groundwater originate from different sources and there is no recognizable hydraulic inter-connection between the aquifers:

- Lithological setting* the alluvial aquifers (i.e. UAA and LAA) flow in unconsolidated coarse-grained alluvium, ranging from gravel to silt, which are separated by several meters of mudstone and clay layers. The HRA is located below the alluvial aquifers and their hydraulic connection is interrupted by several meters of Si-cemented conglomerate (Fig. 2b).
- Hydraulic properties* the piezometric level in the HRA geotechnical boreholes is higher than the water table in the LAA. The HRA is consequently a confined fractured aquifer, where the overburdened lithostatic pressure and the compressibility of water have caused it to become a non-flowing artesian aquifer (Assari 2019).
- Hydrochemical features* the major and minor ion concentrations in all of the groundwater samples have a

different chemistry relative to modern groundwater in the study area (Figs. 5, 6, 7, 8 and Fig. 9).

- (d) *Stable isotope compositions* the results of $\delta^{18}\text{O}$, $\delta^2\text{H}$, and deuterium excess in UAA, LAA, and HRA suggest that these aquifers originate from different sources (Fig. 10 and Table 2).
- (e) *Age dating of groundwater* all groundwater samples in UAA, LAA, and HRA were tritium-free, and ^{14}C dating attributes the age of these waters to three time-periods: 6200, 18,000, and 27,500 ybp (Fig. 12).

As mentioned earlier, the UAA, LAA, and HRA were formed due to transgression and regression of inland lakes during time-periods with a time interval of about 10,000 years, where during these periods, the large lakes covered the entire area. Nowadays, the salt playas remaining from those periods include the Kheirabad SP in the north, the Qatrouyeh SP in the southwest, and the Marg SP in the southeast. In summary, the change of the lakes can be explained by the following three periods:

- (1) *27,500 ybp-period* During this period, almost the entire area was covered by large inland lakes with high EC contents and a significant amount of alkali elements in the lake water after passing through unconsolidated alluvium and have penetrated into the hard-rock host materials (Fig. 13a). As mentioned above, the dissolution of halite was considered to be the main origin of groundwater salinization in the UAA, LAA, and HRA. However, no signs of evaporative layers were observed in the mining area's geotechnical borehole logs (Assari 2019; Assari and Mohammadi 2017; Babaki and Aftabi 2006; Heidari-Nejad et al. 2017). Therefore, the salt must have dissolved in the surface water before penetrating into the aquifer. The study area is a closed inland basin located in arid and semi-arid climates, and evaporation of water accumulated in the basin has formed thick layers of halite over long periods (as the salt layer is precipitating nowadays in the SP) (Maknoui Gilani 2019; Masoumi et al. 2020). At that time, the water level of the lake was significantly raised for a long time, and the evaporative layers were dissolved in the surface water, forming the HRA water after infiltrating into the ground. At the end of the transgression period, the unconsolidated deposits overlying the HRA consolidated to become the impermeable Si-cement conglomerate strata, and the HRA was hydraulically disconnected from the local hydrological cycle (Jafari et al. 2018; Maknoui Gilani 2019).
- (2) *18,000 ybp-period* During this transgression, the salinity of the infiltrated water ranged from 20,000 to 30,000 $\mu\text{S cm}^{-1}$, leading to the formation of the LAA. The origin of the groundwater and mechanism of salinity

were similar to that of the HRA but much less intense. During this time-period, coinciding with the penetration of water into the LAA, the fine-grained layers (i.e. mudstone and claystone) precipitated as clay lenses (Fig. 13b). Groundwater in the LAA had a significant amount of dissolved Na^+ and reverse exchange between Na^+ and Ca^{2+} occurred in this aquifer, but less abundantly than in the HRA.

- (3) *6200 ybp-period* Several transgressive and regressive cycles occurred between 18,000 and 6000 ybp, and a sequence of coarse-grained and fine-grained alluvial deposits precipitated, indicating that a sequence of high- and low-energy environments dominated the study area. During this period, groundwater was much less saline than during the LAA and HRA, ranging from 5000 to 9000 $\mu\text{S cm}^{-1}$. This showed that the amount of precipitated salt in the basin was likely much less than at 18,000 and 27,500 ybp. Rock-water interactive processes have not been observed in this aquifer, the groundwater of which is the only source of salinity attributed to halite dissolution. Groundwater in the UAA and LAA generally flows through buried paleochannels extending NW–SE and W–E. These channels are filled with coarse-grained fan deposits (Fig. 13c; Shafiei et al. 2009).

The depth of the water table in the UAA is ≈ 50 to 60 m below the ground surface. Despite the shallow water depth, there is no hydraulic connection between the aquifer and local meteoric water for two reasons: a) the surface alluvium is significantly fine-grained (fine silt to fine sand) and does not allow rainwater to infiltrate into the aquifer, and b) the potential evaporation was reported to be more than 2,800 mm in a year, while the average annual precipitation was only 170 mm year⁻¹ (Maknoui Gilani 2019; Maknoui et al. 2018).

Summary and Conclusion

This study identified the origin of the groundwater and sources of salinity in a multi-layered alluvial-hard rock aquifer system. Identifying the origin of groundwater in a complex aquifer system requires an integrated approach including geological, hydrogeological, and hydrochemical methods with isotopic measurements and age dating to minimize the uncertainty of the individual approaches. The results showed that Na-Cl is the dominant water type throughout the study area, which was indicated by the low Cl/HCO_3 and Cl/SO_4 weight ratios in the KhA and UAA, and high weight ratios in the LAA and HRA. The TDS of the groundwater ranged from a minimum of 1.1 g L⁻¹ in the KhA to > 148 g L⁻¹ in the brines of the HRA.

Results highlighted halite dissolution as the main origin of salinity in groundwater samples. Moreover, the groundwater of the HRA and LAA is likely affected by reverse cation exchange as well as dissolution of sulfate and carbonate minerals observed in KhA and UAA. Stable isotopes of KhA samples were closest to LMWL. No evidence of $\delta^{18}\text{O}$ and $\delta^2\text{H}$ analyses and age dating supported saline water intrusion from the SP to the mines. However, our results revealed that the UAA, LAA, and HRA groundwater samples were related to the time-periods of 27,500, 18,000, and 6200 ybp, suggesting that the groundwater flowing in these aquifers all originate from different sources.

The developed model of groundwater circulation suggests that alternations of transgression and regression of an inland lake during three time periods (i.e. 27,500, 18,000, and 6200 ybp) created opportunities for ancient meteoric waters to infiltrate into the aquifers during transgression periods. Therefore, during the beginning of the regressive periods, the hydrogeological conditions of the aquifers and the rapid circulation of meteoric water were interrupted by the diagenesis of impermeable clastic sedimentary rocks.

Supplementary Information The online version contains supplementary material available at <https://doi.org/10.1007/s10230-022-00902-6>.

Acknowledgements This research was carried out at Shiraz University and partly supported by the Research and Development Division of the Gohar-Zamin Iron Ore Company. The authors would like to thank the four anonymous reviewers and the Editor-in-Chief for their constructive comments and suggestions.

References

- Abirifard M, Raeisi E, Zarei M, Zare M, Filippi M, Bruthans J, Talbot CJ (2017) Jahani Salt Diapir, Iran: hydrogeology, karst features and effect on surroundings environment. *Int J Speleol* 46(3):445–457. <https://doi.org/10.5038/1827-806X.46.3.2133>
- Ahmadi S, Jahanshahi R, Moeyni V, Mali S (2018) Assessment of hydrochemistry and heavy metals pollution in the groundwater of Ardestan mineral exploration area, Iran. *Environ Earth Sci* 77(5):1–13. <https://doi.org/10.1007/s12665-018-7393-7>
- Ait Brahim Y, Benkaddour A, Agoussine M, Ait Lemkademe A, Yacoubi L, Bouchaou L (2015) Origin and salinity of groundwater from interpretation of analysis data in the mining area of Oumjane, Southeastern Morocco. *Environ Earth Sci* 74(6):4787–4802. <https://doi.org/10.1007/s12665-015-4467-7>
- Alçiçek H, Bülbül A, Brogi A, Liotta D, Ruggieri G, Capezzuoli E, Meccheri M, Yavuzer İ, Alçiçek MC (2018) Origin, evolution and geothermometry of the thermal waters in the Gölemezli geothermal field, Denizli Basin (SW Anatolia, Turkey). *J Volcanol Geotherm Res* 349:1–30. <https://doi.org/10.1016/j.jvolgeores.2017.07.021>
- Argamasilla M, Barberá JA, Andreo B (2017) Factors controlling groundwater salinization and hydrogeochemical processes in coastal aquifers from southern Spain. *Sci Total Environ* 580:50–68. <https://doi.org/10.1016/j.scitotenv.2016.11.173>
- Assari A (2019) Defining hydrogeology of the Gohar-Zamin open pit mine, Iran: a case study in a hard-rock aquifer. *Hydrogeol J* 27(4):1479–1495. <https://doi.org/10.1007/s10040-018-01919-4>
- Assari A, Mohammadi Z (2017) Combined use of geostatistics and multi-criteria decision analysis to determine new pumping well locations in the Gol-Gohar open pit mine, Iran. *Mine Water Environ* 36(2):283–298. <https://doi.org/10.1007/s10230-017-0442-8>
- Babaki A, Aftabi AJ (2006) Investigation on the model of iron mineralization at Gol Gohar iron deposit, Sirjan-Kerman. *Geosci J* 61:40–59 (in Persian)
- Bagheri R, Nadri A, Raeisi E, Kazemi GA, Eggenkamp HGM, Montaseri A (2014a) Origin of brine in the Kangan gasfield: isotopic and hydrogeochemical approaches. *Environ Earth Sci* 72(4):1055–1072. <https://doi.org/10.1007/s12665-013-3022-7>
- Bagheri R, Nadri A, Raeisi E, Shariati A, Mirbagheri M, Bahadori F (2014b) Chemical evolution of a gas-capped deep aquifer, south-west of Iran. *Environ Earth Sci* 71(7):3171–3180
- Baudron P, Alonso-Sarría F, García-Aróstegui JL, Cánovas-García F, Martínez-Vicente D, Moreno-Brotóns J (2013) Identifying the origin of groundwater samples in a multi-layer aquifer system with Random Forest classification. *J Hydrol* 499:303–315. <https://doi.org/10.1016/j.jhydrol.2013.07.009>
- Belkhiri L, Mouni L, Boudoukha A (2012) Geochemical evolution of groundwater in an alluvial aquifer: case of El Eulma aquifer, East Algeria. *J Afr Earth Sci* 66–67:46–55. <https://doi.org/10.1016/j.jafrearsci.2012.03.001>
- Boschetti T, Angulo B, Cabrera F, Vásquez J, Montero RL (2016) Hydrogeochemical characterization of oilfield waters from south-east Maracaibo Basin (Venezuela): diagenetic effects on chemical and isotopic composition. *Mar Pet Geol* 73:228–248. <https://doi.org/10.1016/j.marpetgeo.2016.02.020>
- Bourke SA, Harrington GA, Cook PG, Post VE, Dogramaci S (2014) Carbon-14 in streams as a tracer of discharging groundwater. *J Hydrol* 519:117–130. <https://doi.org/10.1016/j.jhydrol.2014.06.056>
- Chen L, Ma T, Du Y, Yang J, Liu L, Shan H, Liu C, Cai H (2014) Origin and evolution of formation water in North China Plain based on hydrochemistry and stable isotopes (2H , 18O , 37Cl and 81Br). *J Geochem Explor* 145:250–259. <https://doi.org/10.1016/j.gexplo.2014.07.006>
- Chen J, Qian H, Gao Y, Wang H, Zhang M (2020) Insights into hydrological and hydrochemical processes in response to water replenishment for lakes in arid regions. *J Hydrol* 581:124386
- Clark ID, Fritz P (2011) Environmental isotopes. In: *Environmental isotopes in hydrogeology*, Part 3, pp 261–262. https://doi.org/10.1007/978-90-481-2642-2_137
- D'Amore F, Panichi C (1985) Geochemistry in geothermal exploration. *Int J Energy Res* 9(3):277–298. <https://doi.org/10.1002/er.4440090307>
- Dansgaard W (1964) Stable isotopes in precipitation. *Tellus* 16(4):436–468. <https://doi.org/10.3402/tellusa.v16i4.8993>
- Dor N, Syafalni S, Abustan I, Rahman MTA, Nazri MAA, Mostafa R, Mejus L (2011) Verification of Surface- Groundwater Connectivity in an Irrigation Canal Using Geophysical, Water Balance and Stable Isotope Approaches. *Water Resour Manag* 25(11):2837–2853. <https://doi.org/10.1007/s11269-011-9841-y>
- Eggenkamp HGM, Louvat P, Agrinier P, Bonifacie M, Bekker A, Krupenik V, Griffioen J, Horita J, Brocks JJ, Bagheri R (2019) The bromine and chlorine isotope composition of primary halite deposits and their significance for the secular isotope composition of seawater. *GCA J* 264:13–29
- Eissa MA, Shawky H, Samy A, Khalil MMH, El Malky M (2018) Geochemical and Isotopic evidence of groundwater salinization processes in El Dabaa area, northwestern coast, Egypt. *Geosci J* 8(11):392
- Gharaat MJ, Mohammadi Z, Rezaeezhad F (2020) Distribution and origin of potentially toxic elements in a multi-aquifer system. *Environ Sci Pollut Res*. <https://doi.org/10.1007/s11356-020-10223-2>

- Gue AE, Mayer B, Grasby SE (2015) Origin and geochemistry of saline spring waters in the Athabasca oil sands region, Alberta, Canada. *Appl Geochem* 61:132–145. <https://doi.org/10.1016/j.apgeochem.2015.05.015>
- Heidari-Nejad H, Zarei M, Merkel BJ (2017) Evaluating the origin of seepage water in the Golgohar iron mine, Iran. *Mine Water Environ* 36(4):583–596. <https://doi.org/10.1007/s10230-017-0447-3>
- Huang L, Deng CB, Huang N, Huang XJ (2013) Multivariate statistical approach to identify heavy metal sources in agricultural soil around an abandoned Pb-Zn mine in Guangxi Zhuang Autonomous Region, China. *Environ Earth Sci* 68(5):1331–1348. <https://doi.org/10.1007/s12665-012-1831-8>
- Jafari A, Karimpour MH, Mazaheri SA, Malekzadeh Shafaroudi A, Askari M (2018) Mineralogy, the nature of magmatic and tectonic setting of amphibolite protolith from Gol Gohar iron ore deposit, Sirjan Kerman. *Iran J Petrol* 9(3):27–54
- Jahanshahi R, Zare M (2015) Assessment of heavy metals pollution in groundwater of Golgohar iron ore mine area. *Iran Environ Earth Sci* 74(1):505–520. <https://doi.org/10.1007/s12665-015-4057-8>
- Jahanshahi R, Zare M (2017) Delineating the origin of groundwater in the Golgohar Mine area of Iran using stable isotopes of 2H and 18O and hydrochemistry. *Mine Water Environ* 36(4):550–563. <https://doi.org/10.1007/s10230-017-0444-6>
- Karolytė R, Serno S, Johnson G, Gilfillan SMV (2017) The influence of oxygen isotope exchange between CO₂ and H₂O in natural CO₂-rich spring waters: implications for geothermometry. *Appl Geochem* 84:173–186. <https://doi.org/10.1016/j.apgeochem.2017.06.012>
- Khaska M, La Salle CLG, Lancelot J, Mohamad A, Verdoux P, Noret A, Simler R (2013) Origin of groundwater salinity (current seawater vs. saline deep water) in a coastal karst aquifer based on Sr and Cl isotopes. Case study of the La Clape massif (southern France). *Appl Geochem* 37:212–227
- Knapton JR (1985) Field guidelines for collection, treatment, and analysis of water samples, Montana District. USGS
- Kouchekezadeh A, Zarei M (2017) Introducing hydrochemical diagnostic tools to differentiate sources of salinity, southern Iran. *Int J Water* 11(3):226–250. <https://doi.org/10.1504/IJW.2017.085880>
- Li P, Wu J, Tian R, He S, He X, Xue C, Zhang K (2018) Geochemistry, Hydraulic connectivity and quality appraisal of multilayered groundwater in the Hongdunzi coal mine, northwest China. *Mine Water Environ* 37(2): 222–237. <https://doi.org/10.1007/s10230-017-0507-8>
- Li C, Gao X, Liu Y, Wang Y (2019a) Impact of anthropogenic activities on the enrichment of fluoride and salinity in groundwater in the Yuncheng Basin constrained by Cl/Br ratio, δ¹⁸O, δ²H, δ¹³C and δ⁷Li isotopes. *J Hydrol* 579: 124211. <https://doi.org/10.1016/j.jhydrol.2019.124211>
- Li P, Tian R, Liu R (2019b) Solute geochemistry and multivariate analysis of water quality in the Guohua phosphorite Mine, Guizhou Province, China. *Expos Health* 11(2): 81–94. <https://doi.org/10.1007/s12403-018-0277-y>
- Maknoui S, Zare M, Raeisi E (2018) Determining the hard rock groundwater pathway in Golgohar complex formation using hydrochemical data in AHP. *Arab J Geosci*. <https://doi.org/10.1007/s12517-018-3472-z>
- Maknoui Gilani S (2019) Design of flood drainage in Golgohar Iron Ore Mine #3. *Hydro Sci Mar Eng* 1(1):15–21. <https://doi.org/10.30564/hsme.v1i1.1255>
- Masoumi I, Kamali G, Asghari O, Emery X (2020) Assessing the impact of geologic contact dilution in ore/waste classification in the Gol-Gohar iron ore mine, southeastern Iran. *Minerals* 10(4):336. <https://doi.org/10.3390/min10040336>
- Mohammadi Z (2009) Assessing hydrochemical evolution of groundwater in limestone terrain via principal component analysis. *Environ Earth Sci* 59(2):429–439. <https://doi.org/10.1007/s12665-009-0041-5>
- Mohammadi Z, Zare M, Sharifzade B (2012) Delineation of groundwater salinization in a coastal aquifer, Bousheher, south of Iran. *Environ Earth Sci* 67(5):1473–1484
- Montcoudiol N, Molson J, Lemieux JM (2015) Géochimie des eaux souterraines en Outaouais (Québec, Canada): une étude à échelle régionale. *Hydrogeol J* 23(2):377–396. <https://doi.org/10.1007/s10040-014-1190-5>
- Nekouei E, Zarei M, Raeisi E (2016) The influence of diapir brine on groundwater quality of surrounding aquifers, Larestan, Iran. *Environ Earth Sci* 75(7):571. <https://doi.org/10.1007/s12665-015-5237-2>
- Owen DDR, Cox ME (2015) Hydrochemical evolution within a large alluvial groundwater resource overlying a shallow coal seam gas reservoir. *Sci Total Environ* 523:233–252. <https://doi.org/10.1016/j.scitotenv.2015.03.115>
- Prasanna MV, Praveena SM, Chidambaram S, Nagarajan R, Elayaraja A (2012) Evaluation of water quality pollution indices for heavy metal contamination monitoring: a case study from Curtin Lake, Miri City, East Malaysia. *Environ Earth Sci* 67(7):1987–2001. <https://doi.org/10.1007/s12665-012-1639-6>
- Qiao W, Li W, Zhang S, Niu Y (2019) Effects of coal mining on the evolution of groundwater hydrogeochemistry. *Hydrogeol J* 27(6):2245–2262. <https://doi.org/10.1007/s10040-019-01969-2>
- Scheiber L, Ayora C, Vázquez-Suñé E, Cendón DI, Soler A, Custodio E, Baquero JC (2015) Recent and old groundwater in the Niebla-Posadas regional aquifer (southern Spain): implications for its management. *J Hydrol* 523:624–635. <https://doi.org/10.1016/j.jhydrol.2015.01.076>
- Scheiber L, Ayora C, Vázquez-Suñé E, Cendón DI, Soler A, Baquero JC (2016) Origin of high ammonium, arsenic and boron concentrations in the proximity of a mine: natural vs. anthropogenic processes. *Sci Total Environ* 541:655–666. <https://doi.org/10.1016/j.scitotenv.2015.09.098>
- Shafiei B, Haschke M, Shahabpour J (2009) Recycling of orogenic arc crust triggers porphyry Cu mineralization in Kerman Cenozoic arc rocks, southeastern Iran. *Miner Depos* 44(3):265–283. <https://doi.org/10.1007/s00126-008-0216-0>
- Soltaninejad A, Ranjbar H, Honarmand M, Dargahi S (2018) Evaporite mineral mapping and determining their source rocks using remote sensing data in Sirjan playa, Kerman, Iran. *Carbonate Evaporite* 33(2):255–274. <https://doi.org/10.1007/s13146-017-0339-4>
- Su Z, Wu J, He X, Elumalai V (2020) Temporal changes of groundwater quality within the groundwater depression cone and prediction of confined groundwater salinity using Grey Markov Model in Yinchuan area of northwest China. *Expos Health* 12(3):447–468. <https://doi.org/10.1007/s12403-020-00355-8>
- Wang Y, Jiao JJ (2012) Origin of groundwater salinity and hydrogeochemical processes in the confined Quaternary aquifer of the Pearl River Delta, China. *J Hydrol* 438–439:112–124. <https://doi.org/10.1016/j.jhydrol.2012.03.008>
- Wen X, Lu J, Wu J, Lin Y, Luo Y (2019) Influence of coastal groundwater salinization on the distribution and risks of heavy metals. *Sci Total Environ* 652:267–277. <https://doi.org/10.1016/j.scitotenv.2018.10.250>
- Yu H, Ma T, Du Y, Chen L (2019) Genesis of formation water in the northern sedimentary basin of South China Sea: clues from hydrochemistry and stable isotopes (D, ¹⁸O, ³⁷Cl and ⁸¹Br). *J Geochem Explor* 196:57–65. <https://doi.org/10.1016/j.gexp.2018.08.005>
- Yuan J, Xu F, Deng G, Tang Y, Li P (2017) Hydrogeochemistry of Shallow groundwater in a karst aquifer system of Bijie City, Guizhou Province. *Water* 9(8):625. <https://doi.org/10.3390/w9080625>

- Zarei M, Raeisi E, Mahmoudi K (2014) The impact of salt diapirs on the quality of carbonate karst waters, Bastak, Iran. *Environ Earth Sci* 71(9):3893–3906. <https://doi.org/10.1007/s12665-013-2775-3>
- Zhao Q, Su X, Kang B, Zhang Y, Wu X, Liu M (2017) A hydrogeochemistry and multi-isotope (Sr, O, H, and C) study of groundwater salinity origin and hydrogeochemical processes in the shallow confined aquifer of northern Yangtze River downstream coastal plain, China. *Appl Geochem* 86:49–58

Springer Nature or its licensor holds exclusive rights to this article under a publishing agreement with the author(s) or other rightsholder(s); author self-archiving of the accepted manuscript version of this article is solely governed by the terms of such publishing agreement and applicable law.